NeuroImage 201 (2019) 116039

Contents lists available at ScienceDirect

NeuroImage

journal homepage: www.elsevier.com/locate/neuroimage

The multipole approach for EEG forward modeling using the finite element method

Johannes Vorwerk [a,b,*,1], Anne Hanrath [d,1], Carsten H. Wolters [b,c], Lars Grasedyck [d]

[a] Institute of Electrical and Biomedical Engineering, UMIT - Private University for Health Sciences, Medical Informatics and Technology, Hall in Tirol, Austria
[b] Institute for Biomagnetism and Biosignalanalysis, University of Münster, Münster, Germany
[c] Otto Creutzfeldt Center for Cognitive and Behavioral Neuroscience, University of Münster, Münster, Germany
[d] Institut für Geometrie und Praktische Mathematik, RWTH Aachen, Aachen, Germany

ARTICLE INFO

Keywords:
EEG
Source analysis
Finite element method
Source modeling
Quadrupole
Multipole

ABSTRACT

For accurate EEG forward solutions, it is necessary to apply numerical methods that allow to take into account the realistic geometry of the subject's head. A commonly used method to solve this task is the finite element method (FEM). Different approaches have been developed to obtain EEG forward solutions for dipolar sources with the FEM. The St. Venant approach is frequently applied, since its high numerical accuracy and stability as well as its computational efficiency was demonstrated in multiple comparison studies. In this manuscript, we propose a variation of the St. Venant approach, the multipole approach, to improve the numerical accuracy of the St. Venant approach even further and to allow for the simulation of additional source scenarios, such as quadrupolar sources. Exploiting the multipole expansion of electric fields, we demonstrate that the newly proposed multipole approach achieves even higher numerical accuracies than the St. Venant approach in both multi-layer sphere and realistic head models. Additionally, we exemplarily show that the multipole approach allows to not only simulate dipolar but also quadrupolar sources.

1. Introduction

Electroencephalography (EEG) is a frequently used tool to observe brain activity in both neuroscience and clinical applications, since it provides a unique time resolution in the millisecond range. In many of these applications, it is desirable to perform EEG source analysis, i.e., to reconstruct the active brain areas evoking a measured signal. To achieve this reconstruction it is necessary to simulate the EEG signal that is generated by activity in a certain region of the brain. This task is called the EEG forward problem (Brette and Destexhe, 2012).

The EEG forward problem can only be solved analytically in simple geometries, such as multi-layer sphere models (de Munck et al., 1988; de Munck and Peters, 1993). To realistically model the subject's head, the use of numerical techniques such as boundary element methods (BEM, Gramfort et al., 2010), finite volume methods (FVM, Cook and Koles, 2006), finite difference methods (FDM, Vatta et al., 2009; Montes-Restrepo et al., 2014), or finite element methods (FEM, Wolters et al., 2007a) is necessary. For all these techniques, the major challenge is to deal with the strong singularity caused by the assumption of a dipolar source to represent brain activity, as it is common in EEG source analysis (de Munck et al., 1988; Hämäläinen et al., 1993; Sarvas, 1987).

Two classes of approaches to solve this problem when applying FEM exist: In the subtraction approach (Wolters et al., 2007b; Engwer et al., 2017), the dipolar source is subtracted from the original equation by using the analytical solution for an infinite, homogeneous volume conductor. Subsequently, a correction potential that accounts for the inhomogeneous conductivity distribution within the head is computed, and the EEG forward solution is obtained by summing up analytical solution and correction potential. In the direct approaches, such as St. Venant (Buchner et al., 1997), partial integration (Yan et al., 1991), and Whitney approach (Tanzer et al., 2005; Pursiainen et al., 2011), the dipole source is approximated by a discrete distribution of current sinks and sources placed on the vertices of the finite element mesh. Each of the approaches follows a different assumption to select these vertices and to determine the strength of the sinks and sources.

Whereas all of these approaches lead to accurate EEG forward

* Corresponding author. Institute of Electrical and Biomedical Engineering, UMIT - Private University for Health Sciences, Medical Informatics and Technology, Hall in Tirol, Austria.
E-mail address: johannes.vorwerk@umit.at (J. Vorwerk).
[1] The first two authors contributed equally to this work.

https://doi.org/10.1016/j.neuroimage.2019.116039
Received 21 February 2019; Received in revised form 14 June 2019; Accepted 19 July 2019
Available online 29 July 2019

simulations, comparison studies between subtraction and direct approaches have shown that the direct approaches have a much lower computational complexity (Bauer et al., 2015; Lew et al., 2009). Thus, a multitude of EEG forward solutions, as needed in many EEG source analysis approaches, can be obtained in a much shorter time. Among the direct approaches, the St. Venant approach was shown to lead to the most accurate results for sources with arbitrary positions and directions in simulation studies in both spherical and realistic head models. As a result, the St. Venant approach has been chosen as forward approach in a variety of simulation (e.g., Güllmar et al., 2010; Cho et al., 2015) and experimental studies (e.g., Aydin et al., 2014; Rullmann et al., 2009).

In this study, we propose to modify the formulation of the St. Venant approach based on the multipole expansion of electric fields. This new formulation leads to reduced numerical errors especially for eccentric sources, whereas the computational effort remains nearly unchanged. Furthermore, it allows to model quadrupolar sources, which is an important advantage over existing FEM approaches, since recent studies have shown that the inclusion of higher order sources may improve source localization for both EEG (Riera et al., 2012) and MEG (Jerbi et al., 2004, 2002; Mosher et al., 1999; Nolte and Curio, 1997). Besides, quadrupolar sources also occur in the diagnosis of spinal chord disorders (Tomori et al., 2010; Sumiya et al., 2017; Ishii et al., 2012).

2. Theory

Assuming the quasi-static approximation of Maxwell's equations (Brette and Destexhe, 2012), the EEG forward problem consists in finding the electric potential $u(\mathbf{x})$ that solves the Poisson equation

$$\nabla \cdot (\sigma \nabla u) = \nabla \cdot \mathbf{j}^p \qquad \text{in } \Omega, \tag{1}$$

$$\sigma \nabla u \cdot \mathbf{n} = 0 \qquad \text{on } \partial\Omega, \tag{2}$$

where Ω is the head domain, $\sigma(\mathbf{x})$ the conductivity distribution of Ω, and $\mathbf{j}^p(\mathbf{x})$ models the electric activity in the brain. In EEG source analysis, a common model for $\mathbf{j}^p$ is the current dipole, $\mathbf{j}^p(\mathbf{x}) = \mathbf{m}\delta_{\mathbf{x}_0}(\mathbf{x})$. The current dipole describes an infinitesimally small current flow at location $\mathbf{x}_0$ with direction $\mathbf{m}$. The current direction $\mathbf{m}$ is called the electric dipole moment.

Given a discretization $\mathcal{T}_h$ of Ω, commonly into tetra- or hexahedra in the 3d case, the FEM for equation (1) can be easily derived (Wolters et al., 2007b; Braess, 2007). However, for the choice of a current dipole as source model, the right-hand side $f = \nabla \cdot \mathbf{j}^p = \nabla \cdot \mathbf{m}\delta_{\mathbf{x}_0}$ is singular, and therefore needs special attention to avoid numerical inaccuracies.

The function f represents the sources and sinks of the current dipole with moment $\mathbf{m}$ at position $\mathbf{x}_0$ and is singular due to the limit case taken in the derivation of the current dipole. In the St. Venant approach (Buchner et al., 1997), the idea is to discretize f using a distribution of sources and sinks placed on certain vertices of the FE mesh that matches certain moments of the dipole source. We propose to refine the St. Venant approach by introducing a different definition of these moments, more specifically of the moments of second order and higher, based on the multipole expansion of electric fields that is well-known from physics (Jackson, 1999).

The basic assumption is identical for the St. Venant and the multipole approaches. First, the positions at which the electrical monopoles are placed are selected. To do so, the vertex $\mathbf{x}_1$ of the discretization $\mathcal{T}_h$ closest to the source position $\mathbf{x}_0$ is determined as well as all vertices $\mathbf{x}_2, \dots, \mathbf{x}_n$ that belong to mesh elements that contain $\mathbf{x}_1$. Thus, the number of vertices is 27 for hexahedral meshes, whereas it is mesh dependent for tetrahedral meshes (commonly larger than 10 in our experiments). To achieve an approximation of the field of the dipole source through this monopole distribution, the strength q_i of sources and sinks at positions $\mathbf{x}_i$ are determined so that the moments of this discrete distribution match those of the original current distribution $\mathbf{j}^p$.

The zeroth moment of the monopole distribution defined by sources and sinks q_i at positions $\mathbf{x}_i$, $\rho = \sum_{i=1}^{n} q_i \delta_{x_i}$, is the sum of charges:

$$M = \sum_{i=1}^{n} q_i. \tag{3}$$

This sum has to be zero for a dipolar source, as there are no monopole contributions to the electric field.

The first moment of the monopole distribution reads

$$\mathbf{p} = \sum_{i=1}^{n} (\mathbf{x}_i - \mathbf{x}_0) q_i = \sum_{i=1}^{n} \Delta\mathbf{x}_i q_i, \tag{4}$$

and corresponds to the dipole moment. These moments are defined identically for the multipole and the St. Venant approaches.

2.1. The St. Venant approach

For the St. Venant approach, the second order moment is defined as (Buchner et al., 1997)

$$Q_k = \sum_{i=1}^{n} q_i \left((\Delta\mathbf{x}_i)_k\right)^2, \quad k = 1, 2, 3. \tag{5}$$

Thus, the St. Venant approach has seven parameters to describe the dipole source when using a second-order approximation, one from (3), three from (4), and three from (5). It is easy to see that this definition does not correspond to the second moment of the multipole expansion of electric fields that is known from physics (Jackson, 1999). This not only prevents the simulation of higher order sources, such as quadrupoles, but might also lead to numerical inaccuracies for dipole sources, since the higher-order contributions to the electric fields are not correctly suppressed. We therefore propose to modify the St. Venant approach by using the actual moments resulting from the multipole expansion.

2.2. The multipole approach

For the multipole approach, we define the second order moment according to the multipole expansion of the electrostatic potential (Hanrath, 2019). The multipole expansion is based on a Taylor expansion of the electric field evoked by a charge distribution ρ. In general, the electric potential u evoked by a charge distribution ρ can be computed as

$$u(\mathbf{x}) = \frac{1}{4\pi\varepsilon_0} \int \frac{\rho(\mathbf{x}')}{\|\mathbf{x} - \mathbf{x}'\|_2} d^3\mathbf{x}'. \tag{6}$$

Performing a Taylor expansion of the term $\frac{1}{\|\mathbf{x}-\mathbf{x}'\|_2}$ around the origin, the electric potential can be expressed as an expansion series:

$$u(\mathbf{x}) = \frac{1}{4\pi\varepsilon_0} \left[\frac{1}{\|\mathbf{x}\|_2} \underbrace{\int \rho(\mathbf{x}') d^3\mathbf{x}'}_{monopole} + \sum_i \frac{x_i}{\|\mathbf{x}\|_2^3} \underbrace{\int x_i' \rho(\mathbf{x}') d^3\mathbf{x}'}_{dipole} + \sum_{i,j} \frac{1}{2} \frac{x_i x_j}{\|\mathbf{x}\|_2^5} \underbrace{\int \left(3 x_i' x_j' - \|\mathbf{x}'\|^2 \delta_{i,j}\right) \rho(\mathbf{x}') d^3\mathbf{x}'}_{quadrupole} + \dots \right]. \tag{7}$$

We only spell out the terms up to the second order at this point. For a detailed derivation of the multipole expansion see, for example, Jackson (1999).

Inserting our discrete source distribution, $\rho = \sum_{i=1}^{n} q_i \delta_{x_i}$, in (7), we find that the zeroth (monopole) and first (dipole) moments coincide with the definitions in equations (3) and (4), respectively, whereas the second moments do not. The second moment of the multipole expansion is the quadrupole moment and can be defined as a tensor

$$Q_{k,l} = \sum_{i=1}^{n} q_i \left(3(\Delta\mathbf{x}_i)_k (\Delta\mathbf{x}_i)_l - (\|\Delta\mathbf{x}_i\|_2)^2 \delta_{k,l}\right), \quad k, l = 1, 2, 3, \tag{8}$$

where a subscript index k indicates the k-th entry of the vector $(\Delta\mathbf{x}_i)$. $\delta_{k,l}$

is the Kronecker delta, i.e., $\delta_{k,l} = 1$ if $k = l$ and 0 otherwise, and $\| \cdot \|_2$ stands for the Euclidean norm, i.e., $(||\Delta \mathbf{x}_i||_2)^2 = \sum_{l=1}^{3} (\Delta \mathbf{x}_i)_l^2$.

Since Q is a symmetric tensor with six independent components, this adds three additional parameters to describe the dipole source compared to (5), resulting in 10 determined parameters for the multipole approach.

Introducing higher order moments is straight-forward when following the definition of the multipole expansion.

2.3. Calculation of the monopole loads

We only derive the calculation of the monopole loads for the multipole approach here. First, we scale with a suitable reference length a^{ref}, chosen larger than twice the element edge length so that $\Delta \mathbf{x}_i / a^{ref} < 1$ for all $i = 1, \ldots, n$, and indicate the scaled variables (e.g., distances and moments) with a bar (e.g., $\Delta \bar{\mathbf{x}}_i$, $\bar{M}$, $\bar{\mathbf{p}}$, $\bar{Q}_{k,l}$).

With this definition of the moments, we can express the q_i through a system of linear equations:

$$\underbrace{\begin{bmatrix} \bar{M} \\ (\bar{\mathbf{p}})_1 \\ (\bar{\mathbf{p}})_2 \\ (\bar{\mathbf{p}})_3 \\ \bar{Q}_{1,1} \\ \bar{Q}_{2,2} \\ \bar{Q}_{3,3} \\ \bar{Q}_{1,2} \\ \vdots \end{bmatrix}}_{\bar{t}} = \underbrace{\begin{bmatrix} 1 & \ldots & 1 \\ (\Delta \bar{\mathbf{x}}_1)_1 & \ldots & (\Delta \bar{\mathbf{x}}_n)_1 \\ (\Delta \bar{\mathbf{x}}_2)_1 & \ldots & (\Delta \bar{\mathbf{x}}_n)_2 \\ (\Delta \bar{\mathbf{x}}_3)_1 & \ldots & (\Delta \bar{\mathbf{x}}_n)_3 \\ 3(\Delta \bar{\mathbf{x}}_1)_1^2 - \|\Delta \bar{\mathbf{x}}_1\|_2^2 & \ldots & 3(\Delta \bar{\mathbf{x}}_n)_1^2 - \|\Delta \bar{\mathbf{x}}_n\|_2^2 \\ 3(\Delta \bar{\mathbf{x}}_1)_2^2 - \|\Delta \bar{\mathbf{x}}_1\|_2^2 & \ldots & 3(\Delta \bar{\mathbf{x}}_n)_2^2 - \|\Delta \bar{\mathbf{x}}_n\|_2^2 \\ 3(\Delta \bar{\mathbf{x}}_1)_3^2 - \|\Delta \bar{\mathbf{x}}_1\|_2^2 & \ldots & 3(\Delta \bar{\mathbf{x}}_n)_3^2 - \|\Delta \bar{\mathbf{x}}_n\|_2^2 \\ 3(\Delta \bar{\mathbf{x}}_1)_1 (\Delta \bar{\mathbf{x}}_1)_2 & \ldots & 3(\Delta \bar{\mathbf{x}}_n)_1 (\Delta \bar{\mathbf{x}}_n)_2 \\ \vdots & \ddots & \vdots \end{bmatrix}}_{\bar{X}} \cdot \underbrace{\begin{bmatrix} q_1 \\ q_2 \\ \vdots \\ q_n \end{bmatrix}}_{q} \quad (9)$$

For a dipolar source, we can easily calculate the left-hand side entries, where we have $\bar{M} = 0$, $\bar{p} = \mathbf{m}/a_{ref}$, and $\bar{Q}_{k,l} = 0$.

The derivation of a linear system to calculate the q_i for the St. Venant approach is identical to that of (9). The entries representing the quadrupole moment, $Q_{k,l}$, as defined in (8), have to be replaced by the second-order moments of the St. Venant approach, Q_k, as defined in (5).

Since the number of degrees of freedom n is in general larger than the number of determined parameters on the left-hand side in (9), no unique solution exists. To select a solution with minimal energy, which is a physiologically plausible approach, we define a regularization matrix $\overline{W}$ by $(\overline{W})_{(m,s)} = (\|\Delta \bar{x}_m\|_2)^{r/2} \delta_{m,s}$ for $r = 1$ or $r = 2$ to solve (9). Now, the vector q is the result of minimizing the functional

$$F_\lambda(q) = \|\bar{t} - \bar{X} q\|_2^2 + \lambda \|\overline{W} q\|_2^2 \quad (10)$$

with $\bar{X}_j$ and $\bar{t}_j$ defined as in (9). The first term measures the difference between the original dipole moment and our approximation, whereas the second term penalizes loads of large absolute value $|q_i|$. Thereby, spatially high-frequent, unphysiological sources with large absolute values that do not contribute to the far-field, so-called blind sources, are avoided (Louis, 2013). Furthermore, this additional term ensures the uniqueness of the solution of minimizing F_λ. Increasing the number of known parameters on the left-hand side of (9), as done when introducing the multipole approach, might help to further increase the numerical stability of the equation system.

Differentiation with respect to the q_i yields the solution of the minimization problem:

$$\left(\bar{X}^T \bar{X} + \lambda \overline{W}^T \overline{W}\right) q = \bar{X}^T \bar{t}, \quad (11)$$

and as result for the vector q,

$$q = \left(\bar{X}^T \bar{X} + \lambda \overline{W}^T \overline{W}\right)^{-1} \cdot \bar{X}^T \bar{t}. \quad (12)$$

The choice $r = 2$ for the regularization matrix results in a spatial concentration of loads around the dipole node, since large products $\Delta \bar{\mathbf{x}}_i q_i$ are penalized. The parameter λ should be chosen as small as possible in order to approximate the desired moments accurately, but large enough to avoid indetermination of the linear system.

We define the parameters following the common choices for the St. Venant approach (see Vorwerk et al., 2018; Pursiainen et al., 2016; Lew et al., 2009; Wolters et al., 2007c; Buchner et al., 1997). We include the moments up to the second-order in (9) and define $a^{ref} = 20$ mm, $r = 2$ and $\lambda = 10^{-6}$. These parameters are fixed for both St. Venant and multipole approach and all evaluated tetrahedral and hexahedral models.

3. Methods

3.1. Implementation

We implemented the multipole approach in FieldTrip-SimBio (http://fieldtriptoolbox.org, Vorwerk et al., 2018), based on the already existing implementation of the St. Venant approach. Since it was shown in previous studies that placing monopoles in multiple conductive compartments leads to less accurate results for sources that are close to compartment interfaces, i.e., the gray matter/CSF surface in our study, we chose to exclude all monopole positions that are not in the same conductive compartment as the source, i.e., not in the gray matter compartment, for both the St. Venant and the multipole approach following the ideas of Medani et al. (2015).

3.2. Evaluation

We evaluated the numerical accuracy of the multipole approach in comparison to the St. Venant approach in both spherical and realistic head models. Therefore, we generated four-layer tetrahedral and hexahedral sphere models distinguishing the conductive compartments brain, cerebrospinal fluid (CSF), skull, and skin (see Fig. 1 left, middle). The tetrahedral model was generated using TetGen (http://wias-berlin.de/software/tetgen/, Si, 2004), where we additionally imposed a quality (qc) and volume constraint (vc) to improve the mesh quality. The quality constraint determines the maximum of the ratio between the circumscribed ball and the shortest edge of a tetrahedron. A low value of the quality constraint enforces the construction of well-shaped tetrahedra, the minimal achievable value is about 0.612 (for a regular tetrahedron). Furthermore, to obtain a uniformly high mesh resolution we applied a volume constraint of 1.0, limiting the maximal volume of each tetrahedron to 1 mm^3. The hexahedral model 4layer_sphere_hex was generated using FieldTrip-SimBio, where a node-shift of 0.49, which is the highest value that guarantees that all hexahedra remain convex, was applied to better resolve the sphere geometry (Camacho et al., 1997; Wolters et al., 2007c). The data of the spherical meshes can be found in Tables 1 and 2.

We distributed sources at radii between 2 and 77 mm in 1 mm steps. For each radius, we randomly generated 125 source positions and determined radial and tangential dipole orientations. Thereby, we can obtain statistical distributions of the numerical errors at each radius for varying positions of the source relative to the FE mesh.

Instead of the radius, we indicate the eccentricity of the source locations, i.e., the quotient of the radius of the source position and the brain/CSF interface (78 mm) in percent, in our evaluation. The eccentricity of the most superficial sources in our study is 98.72%. The numerical accuracies at high eccentricities are most relevant in practice, as sources in realistic head models are commonly placed in the gray matter compartment closely to the gray matter/CSF interface. The forward solutions were evaluated at 522 regularly distributed electrode positions on the surface of the models. To calculate the numerical error, we used the analytical solution derived by de Munck and Peters (1993) as reference.

To evaluate the accuracy of the multipole approach in a more realistic

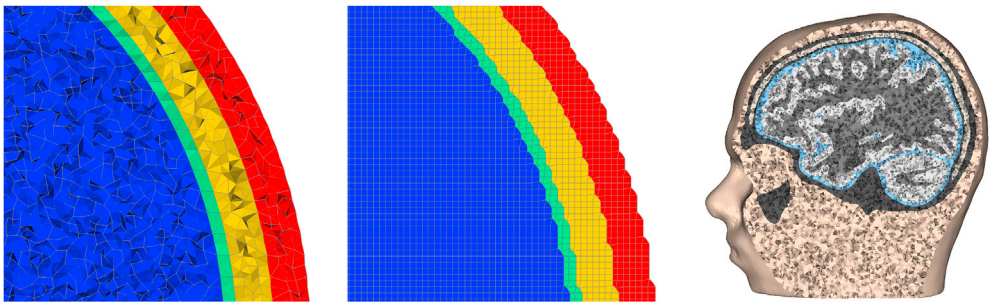

Fig. 1. Visualization of models *4layer_sphere_tet* (left), *4layer_sphere_hex* (middle), and *6layer_realistic* (right).

Table 1
Sphere model.

	Medium	Brain	CSF	Skull	Skin
4-layer	Radius [mm]	78	80	86	92
	Conductivity [S/m]	0.33	1.79	0.01	0.43

Table 2
Parameters of the sphere models.

Model	nodes	elements	qc	vc [mm^3]	node shift
4layer_sphere_tet	801,633	4,985,234	1.0	1.12	-
4layer_sphere_hex	3,342,701	3,262,312	-	-	0.49

scenario, we compared the multipole and the St. Venant approaches in a realistic six-layer tetrahedral head model distinguishing white matter, gray matter, CSF, skull compacta, skull spongiosa, and skin (see Fig. 1, right, Vorwerk et al., 2014). For the comparison, we generated two versions of this head model with different resolutions, i.e., different amounts of mesh vertices and elements, whereas the geometry of the compartment interfaces remained unchanged. Again, the two models were generated using TetGen. The model *6layer_realistic* consisted of 984,569 vertices and 6,107,561 elements and the model *6layer_realistic_hr* consisted of 2,159,337 vertices and 13,636,294 elements. We distributed 129,640 sources regularly on the gray/white matter interface and shifted them into the gray matter, until the node closest to the source position exclusively belonged to gray matter elements. The EEG forward solution was evaluated at 80 electrode positions on the head surface (74 electrodes according to 10-10 system and 6 EOG channels).

In both models, we computed forward solutions for the multipole and the St. Venant approach. For the realistic head model, no exact analytical solution that could be used as reference solution exists. Therefore, a numerical solution obtained in the high-resolution model *6layer_realistic_hr* was used as reference solution. To avoid a bias of our reference solution towards one or the other approach, we created a reference solution by taking the mean of the multipole and the St. Venant solution in model *6layer_realistic_hr* and computed the errors of the multipole and the St. Venant solution in model *6layer_realistic* in comparison to this reference solution.

In all experiments, we used RDM (minimal error 0, maximal error 2) (Meijs et al., 1989) and lnMAG (minimal error 0, maximal error $\pm\infty$) (Güllmar et al., 2010) as error measures:

$$RDM\left(u^{num}, u^{ref}\right) = \left\| \frac{u^{num}}{\|u^{num}\|_2} - \frac{u^{ref}}{\|u^{ref}\|_2} \right\|_2$$
$$lnMAG\left(u^{num}, u^{ref}\right) = \ln\left(\frac{\|u^{num}\|_2}{\|u^{ref}\|_2}\right) \quad (13)$$

u^{num} and u^{ref} denote the numerical and reference solution at the electrode positions, respectively. u^{ref} is the result of the analytical solution derived by de Munck and Peters (1993) in the sphere models and the reference solution derived from the mean of the multipole and St. Venant solution in the high-resolution realistic head model.

The RDM measures changes in the signal topography and the lnMAG measures changes in the overall signal magnitude in comparison to the reference solution. In terms of EEG source analysis, the RDM relates to errors in reconstructed source location and orientation, whereas the lnMAG relates to errors in reconstructed source magnitude. Dannhauer et al. (2011) showed that a higher RDM correlates with a less accurate source localization. Thus, a low RDM is of high importance for almost all applications of EEG source analysis. The lnMAG is only of relevance, if the strength of different reconstructed sources is compared. In such scenarios, a small variance of the lnMAG (across all eccentricities) might be even more important than small absolute values of the lnMAG.

4. Results

4.1. Sphere model studies

Firstly, we evaluated the multipole approach in comparison to the St. Venant approach in both hexahedral and tetrahedral sphere models. Table 3 shows the computation times of a single FE right-hand side for both approaches. We find no significant difference in computation times between multipole and St. Venant approach with an increase of less than 1% in both the tetrahedral and the hexahedral model.

Fig. 2 depicts the numerical accuracies of the multipole and the St. Venant approach in model 4layer_sphere_tet as box-and-whisker plots, i.e., for each eccentricity the black horizontal bar marks the median, the box spans from lower quartile to upper quartile and the whiskers mark minimum and maximum of the error over all sources. For all source positions, the multipole approach leads to smaller RDM and lnMAG errors than the St. Venant approach. We find that especially at the highest eccentricities, the multipole approach leads to smaller errors than the St. Venant approach. A high accuracy at high eccentricities is especially important in practice, since these source positions correspond to the scenario of a source being placed in the gray matter compartment close to the gray matter/CSF interface, as it commonly occurs in realistic head models.

The RDMs for the multipole approach are below 0.015 for all source positions and orientations, whereas the RDMs for the St. Venant approach are up to 0.03 at highest eccentricities. Both the St. Venant and the multipole approach show increasing RDMs with higher eccentricity, but the increase of the RDM for the multipole approach is less strong. Furthermore, the maximal RDM errors for the St. Venant approach increase discontinuously, whereas the increase of the maximal errors for the multipole approach is continuous, demonstrating the increased

Table 3
Computation times for a single right-hand side.

Model	St. Venant	Multipole
4layer_sphere_tet	69.6 ms	70.1 ms
4layer_sphere_hex	82.7 ms	83.0 ms

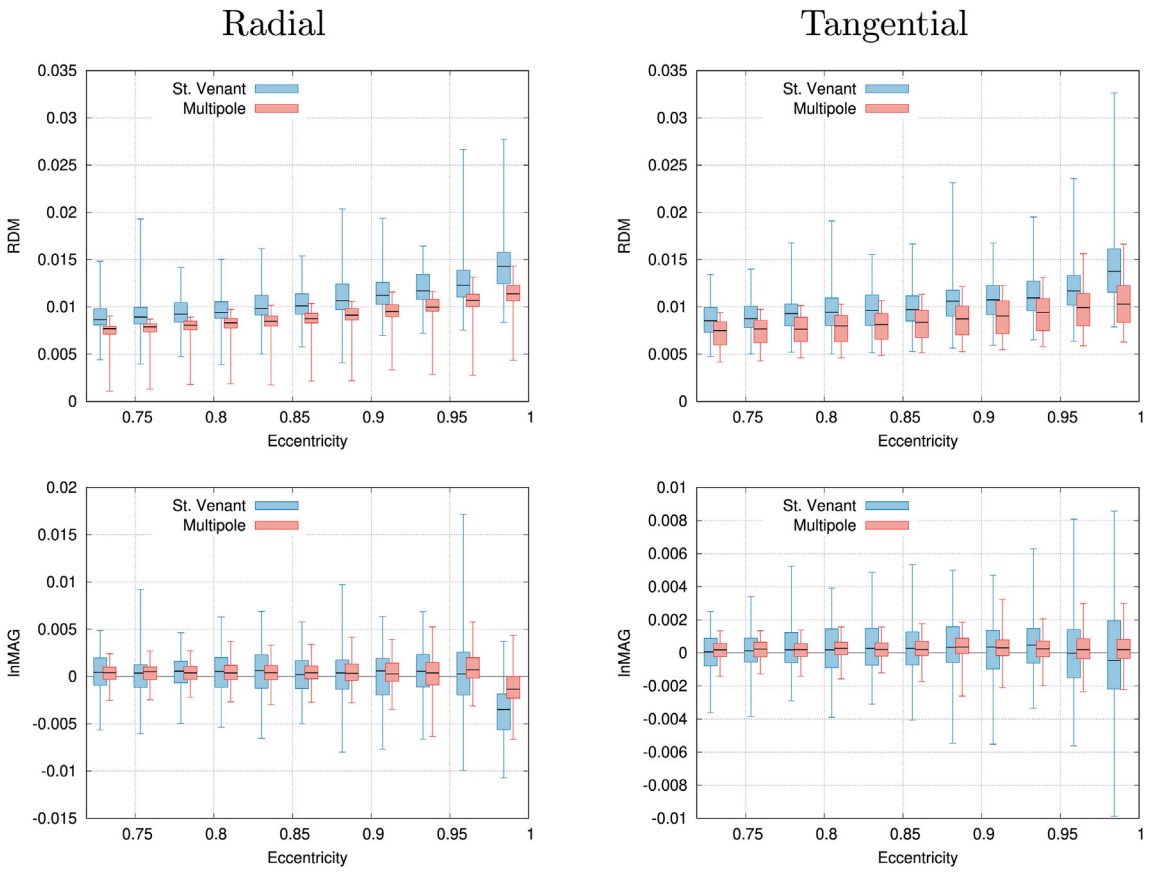

Fig. 2. RDM (top row) and lnMAG (bottom row) for radial (left column) and tangential (right column) source orientations for model 4layer_sphere_tet. For a better readability, the boxes for St. Venant and multipole approach at the same eccentricity are slightly shifted toward a lower and higher eccentricity, respectively.

stability achieved by employing the multipole approach.

The multipole approach leads to smaller absolute values and variance of the lnMAG at all eccentricities. The lnMAG errors for the multipole approach admit maximal absolute values below 0.005 and 0.002 for radial and tangential sources, respectively, whereas the maximal absolute values for the St. Venant approach exceed 0.015 and 0.01, respectively. The variance of the lnMAG is smaller for the multipole approach at all eccentricities. Furthermore, the variance of the lnMAG only slightly increases with higher eccentricity for the multipole approach, whereas the variance increases stronger for the St. Venant approach. The range between minimal and maximal lnMAG over all eccentricities is less than 0.015 and 0.007 for the multipole approach and radial and tangential source orientation, respectively, but more than 0.025 and 0.015 for the St. Venant approach.

For the hexahedral sphere model, the improvements gained through the multipole approach are less clear than in the tetrahedral head model. A small improvement with regard to the RDM is observable at low eccentricities for both radial and tangential sources. However, the errors at these eccentricities are already very low for both St. Venant and multipole approach. For the highest eccentricity, the RDM for both the St. Venant and the multipole approach clearly increases, probably due to the inaccurate representation of the compartment interfaces in the hexahedral models. The RDM errors for St. Venant and multipole approach for tangential sources are almost equal, but the multipole approach leads to smaller RDM errors for highly eccentric radial sources. Small RDM errors for these source positions are important in practice, because sources are commonly placed close to the gray matter/CSF interface, i.e., the cortex surface, and with an orientation normal to the cortex surface, which corresponds to a radial orientation in the sphere model. Also with regard to the lnMAG, both approaches perform essentially identical for all eccentricities but the highest one. For radial sources, the lnMAG for the multipole approach at the highest eccentricity varies strongly compared to lower eccentricities, a behavior that is disadvantageous if the source strength of different reconstructed sources has to be compared. The lnMAG for the St. Venant approach shows less variation. For tangential sources, the multipole approach leads to a slight improvement in lnMAG at the highest eccentricity.

To further demonstrate the improved numerical stability achieved by using the multipole instead of the St. Venant approach, we evaluated the dependency of the numerical errors on the position of the dipole source relative to the mesh elements. For the axis-aligned hexahedral sphere mesh 4layer_sphere_hex with center in the origin, i.e., all edges of hexahedra for which no node-shift was applied are parallel to either the x-, y-, or z-axis of the Cartesian coordinate system, we placed tangential dipoles in the $z = 0.5$ mm plane. The $z = 0.5$ mm plane is parallel to the edges in x- and y-directions and goes through the centers of the elements it cuts. The dipoles are distributed on a grid with a resolution of 0.1 mm in an area of 5.1×5.1 mm. The dipole configuration is visualized in Fig. 4. Through the dense sampling of the dipole positions, it is possible to visualize the dependency of the numerical errors on the position of the dipole inside the grid element. The minimal eccentricity of the sources is 89.75% in the bottom left corner, the maximal eccentricity is 98.00% in the top right corner.

Fig. 5 shows the distributions of RDM and lnMAG for both multipole and St. Venant approach for this source distribution. Besides the numerical errors, we also visualize the boundaries of the mesh elements (gray lines) to be able to estimate the position of the dipole source relative to the mesh element. For the multipole approach, we find a smooth distribution of the errors that increases continuously with the eccentricity (from bottom left to top right). In contrast, for the St. Venant approach we find that the errors clearly depend on the position of the dipole inside the element. Both RDM and lnMAG jump when the node of

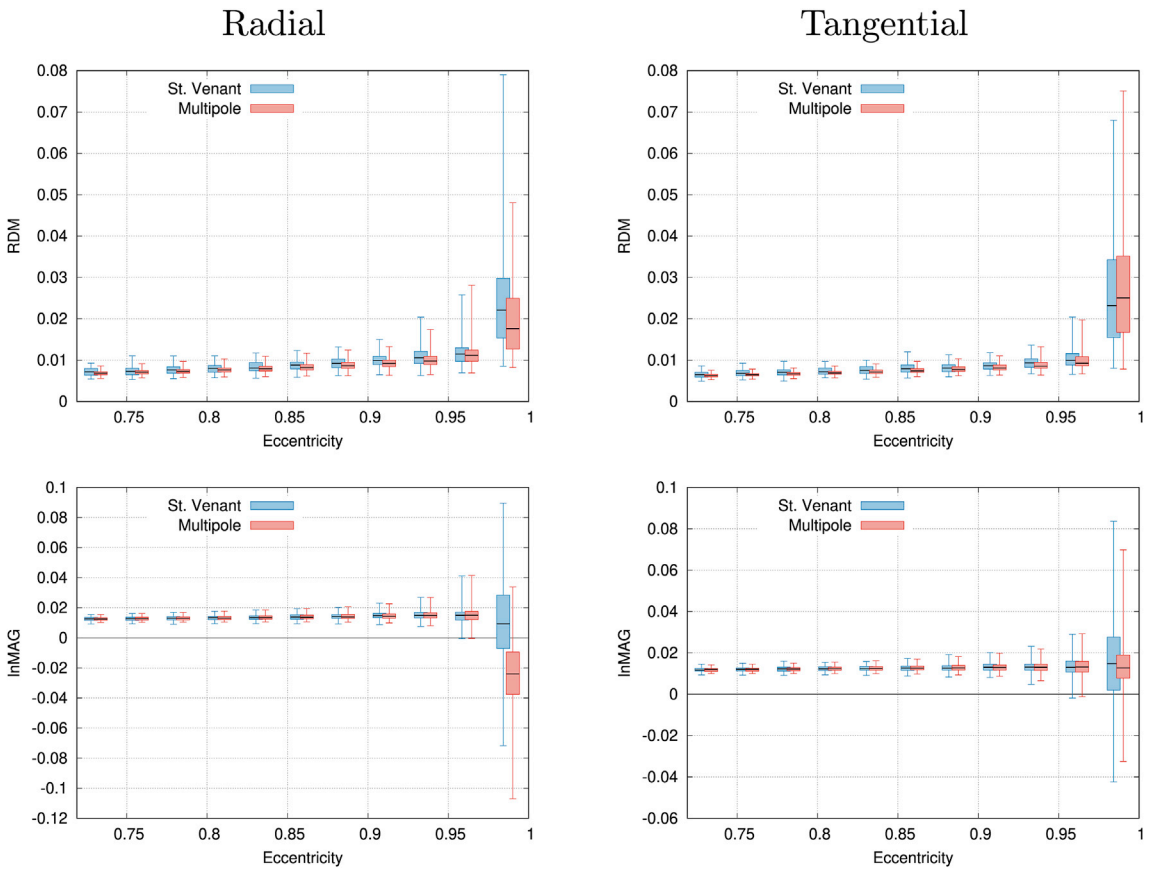

Fig. 3. RDM (top row) and lnMAG (bottom row) for radial (left column) and tangential (right column) source orientations for model 4layer_sphere_hex. For a better readability, the boxes for St. Venant and multipole approach at the same eccentricity are slightly shifted toward a lower and higher eccentricity, respectively.

the FE grid closest to the dipole position changes. Therefore, in practical applications, a careful selection of the dipole position (commonly directly on the nodes of the FE mesh) is advisable to achieve optimal numerical accuracies for the St. Venant approach, whereas such precautions do not seem to be necessary for the multipole approach.

4.2. Realistic head model studies

To estimate the accuracy of St. Venant and multipole approach in a more realistic scenarios, we calculated forward solutions in a realistic head model. Fig. 6 displays the cumulative relative frequency for RDM and lnMAG compared to the reference solution in the realistic head model. The cumulative relative frequency indicates the fraction of sources for which RDM and lnMAG, respectively, lie below a certain value, i.e., the y-value of the curve indicates which fraction of sources has an error smaller than the x-value. Accordingly, the rise of the curve should be as steep as possible for both the RDM and lnMAG and furthermore as close as possible to the $x = 0$ line for the lnMAG. The results in the realistic (tetrahedral) head model (Fig. 6) are in line with the results of the sphere study. Both with regard to RDM and lnMAG, the multipole approach leads to smaller errors than the St. Venant approach (visible through a steeper curve for the RDM and a curve more closely centered around the zero-line for the lnMAG).

To demonstrate the possibility of simulating quadrupolar sources using the multipole approach, we generated a scenario as illustrated in Fig. 7a. This scenario, a "linear quadrupole", represents distributed activity on both sides of a gyrus (gray arrows), which can approximately be represented by two dipolar sources orthogonal to the cortex surface with opposite signs, one for each side of the gyrus (black and red arrows $\mathbf{m}$ and $-\mathbf{m}$ in Fig. 7a). In our idealized scenario of symmetric brain activity with equal source strength on both sides of the gyrus, there would be no resulting EEG signal when simulated as two dipole sources at the same position, since the EEG signals of the two sources are exactly the inverse of each other and cancel out.

However, this source scenario has a non-zero quadrupole moment. The quadrupole moment of such a (unit) source in an orthonormal coordinate system with the dipole direction $\mathbf{m}$ as the first basis vector is diagonal, $Q = \mathrm{diag}(4, -2, -2)$, and can be simulated using the multipole approach.

In practice, it is not realistic that the activity on the two sides of the gyrus (black and red arrows) exactly cancels out, so that a residual dipole moment in addition to the quadrupole moment can be expected. Nevertheless, a scenario as depicted in Fig. 7a cannot be optimally reconstructed when a source space consisting of only dipolar sources is used for source analysis. The multipole approach allows to easily expand the source space with quadrupolar sources to better explain complex, yet not unrealistic, source scenarios in which quadrupolar sources occur.

Fig. 7b and c show the resulting EEG patterns for a dipolar source with moment $\mathbf{m}$ and a quadrupolar source with moment Q, respectively. Three poles (one positive, two negative) are visible when performing a simulation of a superficial, perfectly tangential linear quadrupole in a sphere model with full sensor coverage. Since in our simulation of the quadrupolar source in a realistic head model the source is neither perfectly tangential nor full sensor coverage is given, only one clearly positive and one clearly negative pole are visible within the coverage of the EEG cap. The maximal voltage measured at the head surface for the quadrupolar source is only 4% of the maximum for the dipole source.

5. Discussion

The multipole approach proposed in this study improves the numerical accuracy and stability of FEM EEG forward solutions for both

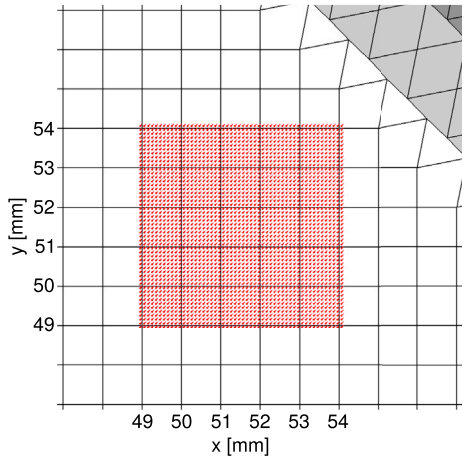

Fig. 4. Dipole distribution used for visualizations in Fig. 5 overlaid on a slice through mesh 4layer_sphere_hex in the z = 0.0 mm plane. Red cones represent dipole positions, black lines represent boundaries of mesh elements. White background represents gray matter elements, light gray background CSF elements, and dark gray background skull elements. Dipoles are placed in the z = 0.5 mm plane, which goes through the center of the hexahedral elements.

tetrahedral and hexahedral finite element meshes and achieves a constantly high accuracy in both spherical and realistic head models. The multipole approach therefore simplifies the use of the FEM in EEG source analysis, as there is no more need to strictly control the placement of sources to achieve optimal numerical accuracies, be it with regard to the position of the dipole source relative to the mesh element (see Fig. 5) or with regard to the distance to the gray matter/CSF interface (see Figs. 2 and 3). Additionally, the multipole approach allows the modeling of quadrupolar sources (see Fig. 7), which can be advantageous not only in MEG and EEG source localization (Jerbi et al., 2004, 2002; Mosher et al., 1999; Nolte and Curio, 1997; Riera et al., 2012), but also in the diagnosis of spinal cord disorders where quadrupolar patterns occur (Tomori et al., 2010; Sumiya et al., 2017; Ishii et al., 2012).

The accuracy, speed, and numerical stability of the St. Venant approach for arbitrary source positions and orientations has been shown in many studies for different spherical and realistic head models, for example in Bauer et al. (2015); Lew et al. (2009) and Vorwerk et al. (2012). In these studies, the St. Venant approach performs superior to other approaches based on the classical continuous Galerkin (CG)-FEM and also when compared to BEM approaches. From our results it can be concluded that the multipole approach outperforms the St. Venant approach in both spherical and realistic tetrahedral head models and therefore most other approaches based on CG-FEM. At the same time, the multipole approach did not lead to a significant increase of computation times in comparison to the St. Venant approach (see Table 3).

In the hexahedral sphere model, the differences between St. Venant and multipole approach are less clear. The numerical errors at high

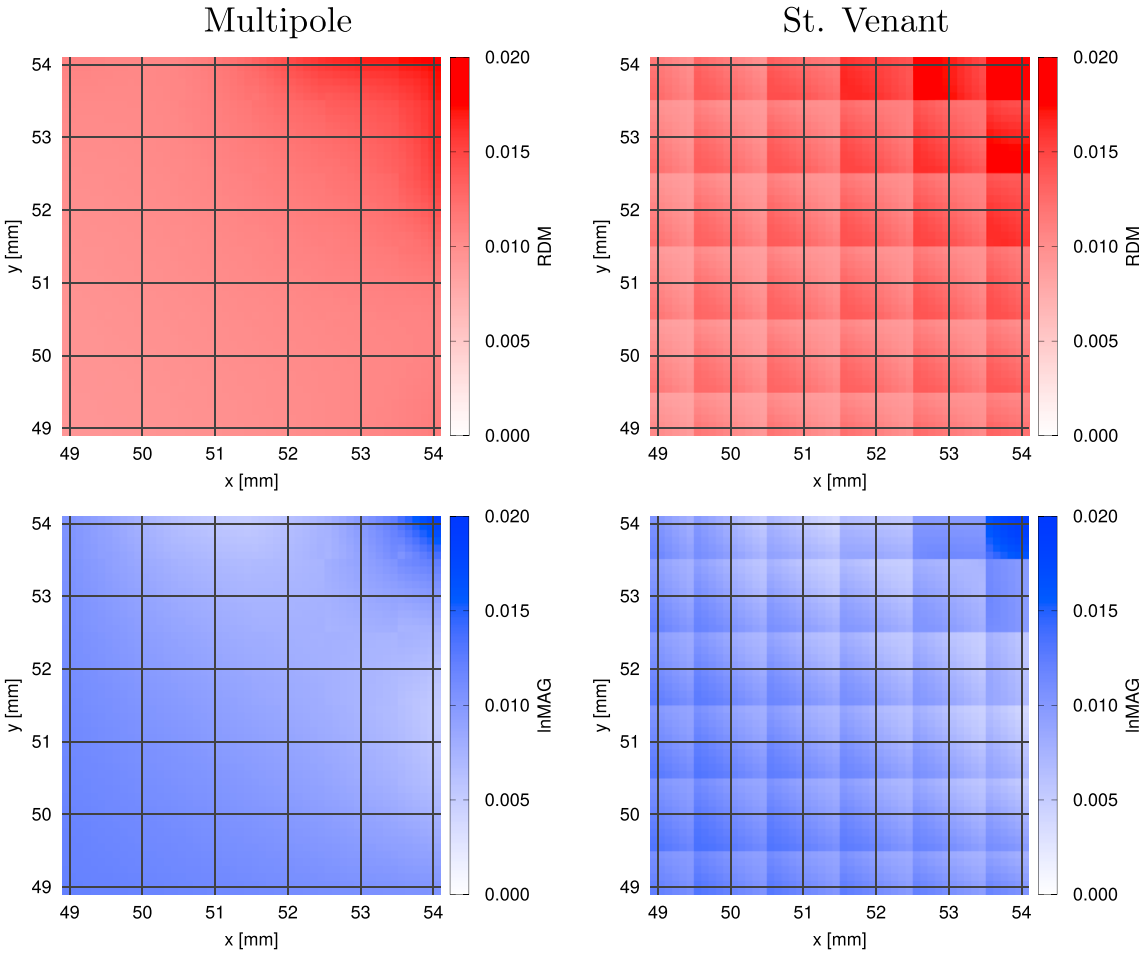

Fig. 5. RDM (top row) and lnMAG (bottom row) for multipole (left column) and St. Venant (right column) approach for tangential dipoles in model 4layer_sphere_hex. Dipoles are placed in the z = 0.5 mm plane and (x, y) ∈ [48.95 mm, 54.05 mm] x [48.95 mm, 54.05 mm] on a grid with a width of 0.1 mm. Dark gray lines visualize the boundaries of the hexahedral mesh elements.

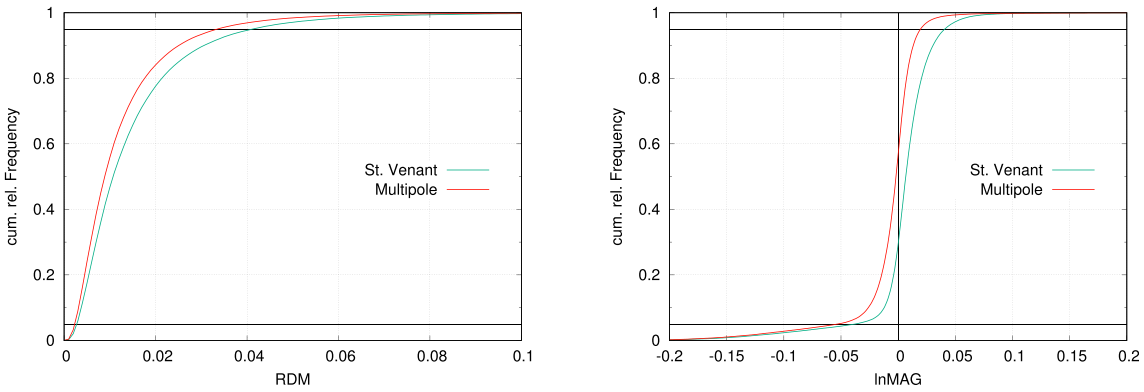

Fig. 6. Cumulative relative frequencies of RDM (left) and lnMAG (right) in realistic head model.

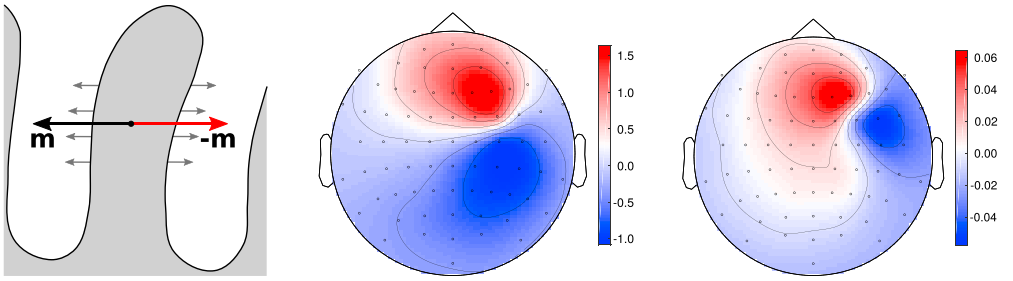

Fig. 7. Schematic illustration of a scenario that creates a quadrupolar source consisting of two dipoles with opposite dipole moments (a) - distributed neural activity on both sides of the gyrus (gray arrows) leads to overall dipole moments **m** and −**m** (black and red arrows), so that the net dipole moment is zero, but a quadrupole moment Q remains. Topoplot of dipolar (b) and quadrupolar (c) source in the somatosensory cortex, simulated in the realistic head model for 10-10 EEG cap. Please observe the difference in color bar range in Subfigures b and c.

eccentricities for both approaches are clearly increased compared to the tetrahedral model, because of the less accurate representation of the compartment boundaries in the hexahedral mesh. An improvement of the numerical accuracy for the multipole approach can be seen only for the topography error RDM for highly eccentric radial sources, which correspond to sources close to the cortex surface with an orientation normal to this surface in realistic head models. This kind of sources appears in many practical applications and a high numerical accuracy for these sources is therefore important. For the same sources, we also find a greater and more variable magnitude error for the multipole approach than for the St. Venant approach. However, this error is less relevant in most practical applications.

Fig. 5 demonstrates the increased numerical stability achieved by the multipole approach. This property allows for a placement of sources without taking into account the position relative to the mesh elements, as it is necessary for the St. Venant approach due to the discontinuous distribution of the numerical errors. Thereby, the generation of source spaces for inverse analysis is simplified, as additional preprocessing steps controlling the position of the source relative to the mesh element can be omitted.

In a recent study, Miinalainen et al. (2019) introduced a novel approach for EEG forward modeling expanding previous work implementing H(div)-conforming source models (Pursiainen et al., 2016, 2011). This approach achieves a higher accuracy than the St. Venant approach at highest eccentricities in spherical head models. However, no numerical errors in a realistic head model have been evaluated so far. Performing a comparison of this approach with the multipole approach, especially in realistic head models, should be a future goal.

For now, the cropping method applied for both St. Venant and multipole approaches to remove monopoles outside the source compartment is very simple, as it removes all invalid nodes from the computed point cloud, in line with the approach introduced by Medani et al. (2015). Though performing well in our study, this might result in removing too many nodes in more complex geometries and leaving equation (9) underdetermined. Therefore, future studies should investigate algorithms that are also able to include new (valid) nodes in the linear system (9) in a second step to prevent an underdetermined linear system.

The ability of the multipole approach to simulate quadrupolar sources has only briefly been demonstrated in this manuscript. Aiming for an application in practice, a thorough evaluation of the accuracy that is achieved for quadrupolar sources is necessary, both in comparison to an analytical solution in sphere models and to the subtraction method for the simulation of quadrupolar sources presented in Beltrachini (2018).

6. Conclusion

We have introduced the multipole approach for EEG forward solutions and demonstrated that it outperforms the established St. Venant approach for dipolar sources in spherical and realistic head models. The implementation of the multipole approach based on existing implementations of the St. Venant approach, such as in FieldTrip, is straightforward. Therefore, it is a future goal to make the multipole approach available for an application in practice. Whereas the modeling of quadrupolar sources might be of great use in a variety of applications, further evaluations of the numerical accuracy are necessary before an application in practice can be recommended.

Funding

This work was supported by the Austrian Wissenschaftsfonds (FWF), project I 3790-B27, the Deutsche Forschungsgemeinschaft (DFG),

projects GR3179/3-1 and WO1425/3-1, 7-1, and by project WO1425/5-2 of the DFG Priority Program 1665.

Appendix A. Supplementary data

Supplementary data to this article can be found online at https://doi.org/10.1016/j.neuroimage.2019.116039.

References

Aydin, Ü., Vorwerk, J., Küpper, P., Heers, M., Kugel, H., Galka, A., Hamid, L., Wellmer, J., Kellinghaus, C., Rampp, S., Wolters, C., 2014. Combining EEG and MEG for the reconstruction of epileptic activity using a calibrated realistic volume conductor model. PLoS One 9 (3), e93154.

Bauer, M., Pursiainen, S., Vorwerk, J., Köstler, H., Wolters, C., 2015. Comparison study for Whitney (Raviart-Thomas)-type source models in finite element method based EEG forward modeling. IEEE (Inst. Electr. Electron. Eng.) Trans. Biomed. Eng. 62 (11), 2648–2656.

Beltrachini, L., 2018. A finite element solution of the forward problem in EEG for multipolar sources. IEEE Trans. Neural Syst. Rehabil. Eng. 27 (3), 368–377.

Braess, D., 2007. Finite Elements: Theory, Fast Solvers and Applications in Solid Mechanics. Cambridge University Press.

Brette, R., Destexhe, A., 2012. Handbook of Neural Activity Measurement. Cambridge University Press, ISBN 978-0-521-51622-8. URL. http://www.di.ens.fr/~brette/HandbookMeasurement/.

Buchner, H., Knoll, G., Fuchs, M., Rienäcker, A., Beckmann, R., Wagner, M., Silny, J., Pesch, J., 1997. Inverse localization of electric dipole current sources in finite element models of the human head. Electroencephalogr. Clin. Neurophysiol. 102, 267–278.

Camacho, D., Hopper, R., Lin, G., Myers, B., 1997. An improved method for finite element mesh generation of geometrically complex structures with application to the skullbase. J. Biomech. 30 (10), 1067–1070.

Cho, J.-H., Vorwerk, J., Wolters, C., Knösche, T., 2015. Influence of the head model on EEG and MEG source connectivity analyses. Neuroimage 110, 60–77.

Cook, M., Koles, Z., 2006. A high-resolution anisotropic finite-volume head model for EEG source analysis. In: Proceedings of the 28th Annual International Conference of the IEEE Engineering in Medicine and Biology Society, vols. 4536–4539.

Dannhauer, M., Lanfer, B., Wolters, C., Knösche, T., 2011. Modeling of the human skull in EEG source analysis. Hum. Brain Mapp. 32 (9), 1383–1399.

de Munck, J., Peters, M., 1993. A fast method to compute the potential in the multisphere model. IEEE (Inst. Electr. Electron. Eng.) Trans. Biomed. Eng. 40 (11), 1166–1174. ISSN 0018-9294.

de Munck, J., van Dijk, B., Spekreijse, H., 1988. Mathematical dipoles are adequate to describe realistic generators of human brain activity. IEEE (Inst. Electr. Electron. Eng.) Trans. Biomed. Eng. 35 (11), 960–966. ISSN 0018-9294.

Engwer, C., Vorwerk, J., Ludewig, J., Wolters, C.H., 2017. A discontinuous Galerkin method to solve the EEG forward problem using the subtraction approach. SIAM J. Sci. Comput. 39 (1), B138–B164.

Gramfort, A., Papadopoulo, T., Olivi, E., Clerc, M., 2010. OpenMEEG: opensource software for quasistatic bioelectromagnetics. Biomed. Eng. Online 9 (1), 45.

Güllmar, D., Haueisen, J., Reichenbach, J., 2010. Influence of Anisotropic Electrical Conductivity in White Matter Tissue on the EEG/MEG Forward and Inverse Solution. A High-Resolution Whole Head Simulation Study, NeuroImage.

Hämäläinen, M., Hari, R., Ilmoniemi, R., Knuutila, J., Lounasmaa, O., 1993. Magnetoencephalography – theory, instrumentation, and applications to noninvasive studies of the working human brain. Rev. Mod. Phys. 65 (2), 413–497. ISSN 1539-0756.

Ishii, S., Kawabata, S., Tomizawa, S., Tomori, M., Sakaki, K., Shinomiya, K., Sekihara, K., Sato, T., Adachi, Y., Okawa, A., 2012. Conductive neuromagnetic fields in the lumbar spinal canal. Clin. Neurophysiol. 123 (8), 1656–1661.

Jackson, J.D., 1999. Classical Electrodynamics, third ed. edn. John Wiley & Sons, New York, NY, ISBN 978-0-471-30932-1.

Jerbi, K., Mosher, J., Baillet, S., Leahy, R., 2002. On MEG forward modelling using multipolar expansions. Phys. Med. Biol. 47 (4), 523.

Jerbi, K., Baillet, S., Mosher, J., Nolte, G., Garnero, L., Leahy, R., 2004. Localization of realistic cortical activity in MEG using current multipoles. Neuroimage 22 (2), 779–793.

Lew, S., Wolters, C., Dierkes, T., Röer, C., MacLeod, R., 2009. Accuracy and run-time comparison for different potential approaches and iterative solvers in finite element method based EEG source analysis. Appl. Numer. Math. 59 (8), 1970–1988.

Louis, A.K., 2013. Inverse und schlecht gestellte Probleme. Springer-Verlag.

Medani, T., Lautru, D., Schwartz, D., Ren, Z., Sou, G., 2015. FEM method for the EEG forward problem and improvement based on modification of the saint venant's method. Prog. Electromagn. Res. 153, 11–22.

Meijs, J., Weier, O., Peters, M., van Oosterom, A., 1989. On the numerical accuracy of the boundary element method. IEEE (Inst. Electr. Electron. Eng.) Trans. Biomed. Eng. 36, 1038–1049.

Miinalainen, T., Rezaei, A., Us, D., Nüßing, A., Engwer, C., Wolters, C.H., Pursiainen, S., 2019. A realistic, accurate and fast source modeling approach for the EEG forward problem. Neuroimage 184, 56–67.

Montes-Restrepo, V., van Mierlo, P., Strobbe, G., Staelens, S., Vandenberghe, S., Hallez, H., 2014. Influence of skull modeling approaches on EEG source localization. Brain Topogr. 27 (1), 95–111.

Mosher, J.C., Leahy, R.M., Shattuck, D.W., Baillet, S., 1999. MEG source imaging using multipolar expansions. In: Biennial International Conference on Information Processing in Medical Imaging, vols. 15–28. Springer.

Nolte, G., Curio, G., 1997. On the calculation of magnetic fields based on multipole modeling of focal biological current sources. Biophys. J. 73 (3), 1253–1262.

Pursiainen, S., Sorrentino, A., Campi, C., Piana, M., 2011. Forward simulation and inverse dipole localization with the lowest order Raviart-Thomas elements for electroencephalography. Inverse Probl. 27 (4).

Pursiainen, S., Vorwerk, J., Wolters, C.H., 2016. Electroencephalography (EEG) forward modeling via H (div) finite element sources with focal interpolation. Phys. Med. Biol. 61 (24), 8502.

Riera, J.J., Ogawa, T., Goto, T., Sumiyoshi, A., Nonaka, H., Evans, A., Miyakawa, H., Kawashima, R., 2012. Pitfalls in the dipolar model for the neocortical EEG sources. J. Neurophysiol. 108 (4), 956–975.

Rullmann, M., Anwander, A., Dannhauer, M., Warfield, S., Duffy, F., Wolters, C., 2009. EEG source analysis of epileptiform activity using a 1mm anisotropic hexahedra finite element head model. Neuroimage 44 (2), 399–410.

Sarvas, J., 1987. Basic mathematical and electromagnetic concepts of the biomagnetic inverse problem. Phys. Med. Biol. 32 (1), 11–22.

Si, H., 2004. TetGen: A Quality Tetrahedral Mesh Generator and Three-Dimensional Delaunay Triangulator, V1.3, User's Manual, Tech. Rep., vol. 9. Weierstrass Institute for Applied Analysis and Stochastics. http://tetgen.berlios.de.

Sumiya, S., Kawabata, S., Hoshino, Y., Adachi, Y., Sekihara, K., Tomizawa, S., Tomori, M., Ishii, S., Sakaki, K., Ukegawa, D., et al., 2017. Magnetospinography visualizes electrophysiological activity in the cervical spinal cord. Sci. Rep. 7 (1), 2192.

Tanzer, O., Järvenpää, S., Nenonen, J., Somersalo, E., 2005. Representation of bioelectric current sources using Whitney elements in finite element method. Phys. Med. Biol. 50, 3023–3039.

Tomori, M., Kawabata, S., Tomizawa, S., Ishii, S., Enomoto, M., Adachi, Y., Sato, T., Shinomiya, K., Okawa, A., 2010. Diagnosis of incomplete conduction block of spinal cord from skin surface using spinal cord evoked magnetic fields. J. Orthop. Sci. 15 (3), 371–380.

Vatta, F., Meneghini, F., Esposito, F., Mininel, F., Di Salle, F., 2009. Solving the forward problem in EEG source analysis by spherical and fdm head modeling: a comparative analysis. Biomed. Sci. Instrum. 45, 382–388.

Vorwerk, J., Clerc, M., Burger, M., Wolters, C., 2012. Comparison of boundary element and finite element approaches to the EEG forward problem. Biomed. Eng. Biomed. Tech. 57 (Suppl. 1), 795–798.

Vorwerk, J., Cho, J.-H., Rampp, S., Hamer, H., Knösche, T., Wolters, C., 2014. A guideline for head volume conductor modeling in EEG and MEG. Neuroimage 100, 590–607.

Vorwerk, J., Oostenveld, R., Piastra, M.C., Magyari, L., Wolters, C.H., 2018. The FieldTrip-SimBio pipeline for EEG forward solutions. Biomed. Eng. Online 17 (1), 37.

Wolters, C., Köstler, H., Möller, C., Härdtlein, J., Anwander, A., 2007a. Numerical approaches for dipole modeling in finite element method based source analysis. Int. Congr. Ser. 1300, 189–192.

Wolters, C., Köstler, H., Möller, C., Härtlein, J., Grasedyck, L., Hackbusch, W., 2007b. Numerical mathematics of the subtraction method for the modeling of a current dipole in EEG source reconstruction using finite element head models. SIAM J. Sci. Comput. 30 (1), 24–45.

Wolters, C., Anwander, A., Berti, G., Hartmann, U., 2007c. Geometry-adapted hexahedral meshes improve accuracy of finite element method based EEG source analysis. IEEE (Inst. Electr. Electron. Eng.) Trans. Biomed. Eng. 54 (8), 1446–1453.

Yan, Y., Nunez, P., Hart, R., 1991. Finite-element model of the human head: scalp potentials due to dipole sources. Med. Biol. Eng. Comput. 29, 475–481.

Hanrath, 2019, Finite Element Representation of the EEG Forward Problem with Multipole Expansion, PhD thesis, RWTH Aachen University, Aachen, Germany. Available from http://www.sci.utah.edu/~wolters/PaperWolters/2019/HanrathDissertation.pdf.